



Macapá, a Brazilian equatorial magnetometer station: installation, data availability, and methods for temperature correction

Cristiano Mendel Martins¹, Katia Jasbinschek Pinheiro³, Achim Ohlert², Jürgen Matzka², Marcos Vinicius da Silva^{2,3}, and Reynerth Pereira da Costa³

¹Geoscience Institute, Universidade Federal do Pará – UFPA, Belém, Brazil

²GFZ German Research Centre for Geosciences, Potsdam, Germany

³Observatório Nacional – MCTI, Geophysics Department, Rio de Janeiro, Brazil

Correspondence: Marcos Vinicius da Silva (mvsilva@gfz-potsdam.de)

Received: 4 July 2023 – Discussion started: 1 February 2024

Revised: 22 May 2024 – Accepted: 16 June 2024 – Published: 30 September 2024

Abstract. In the last 60 years, the largest displacement of the magnetic equator (by about 1100 km northwards) occurred in the Brazilian longitudinal sector. The magnetic equator passed by Tatuoca magnetic observatory (TTB) in northern Brazil in 2012 and continues to move northward. Due to the horizontal geomagnetic field geometry at the magnetic equator, enhanced electric currents in the ionosphere are produced – the so-called equatorial electrojet (EEJ). The magnetic effect of the EEJ is observed in the range of $\pm 3^\circ$ from the magnetic equator, where magnetic observatories record an amplified daily variation of the H component. In order to track the spatial and temporal variation of this phenomena, a new magnetometer station was installed in Macapá (MAA), which is about 350 km northwest of TTB. In this paper, we present the setup and data analysis of MAA station from November 2019 until September 2021. Because of its special configuration, we develop a method for temperature correction of the vector magnetometer data.

vide observations from low Earth orbit. Magnetic observatories produce high-quality and continuous data over long periods (Matzka et al., 2010). Precise and frequent absolute measurements of declination and inclination by trained staff are required to calibrate geomagnetic observatory data. Observatories belonging to INTERMAGNET (International Real-time Magnetic Observatory Network) follow quality standards for measuring and transmitting real-time data (St-Louis et al., 2020). They are an important data source for studies of the internal geomagnetic field and its secular variation and studies of space climate, e.g. with the help of geomagnetic indices. However, there is an uneven spatial distribution of magnetic observatories around the globe, which is worse in the Southern Hemisphere and oceans. There are many reasons for such uneven distribution, such as infrastructure requirements, data transmission problems (especially in remote areas), need for trained staff, and a lack of investments that are fundamental to maintain or construct new observatories. On the other hand, magnetometer stations are not so demanding in terms of infrastructure and staffing requirements. The three components of the magnetic field are measured continuously in a magnetometer station, as is done in the observatories; however, absolute measurements are not periodically acquired. Typically, magnetometer stations are intended to monitor the external and induced geomagnetic fields. They can also be used as a first step to investigate the suitability of a new location before constructing a geomagnetic observatory.

In Brazil, there are two INTERMAGNET observatories: one in Vassouras (VSS – Rio de Janeiro, RJ) and another in

1 Introduction

With globally distributed geomagnetic observations it is possible to investigate the different geomagnetic field sources in the core (the largest part of the measured field), crust, ionosphere, magnetosphere, and induced fields (Hulot et al., 2010). Temporal variations in the Earth's magnetic field at ground level are monitored by geomagnetic observatories (Matzka et al., 2010) and magnetometer stations (Chulliat et al., 2017). Dedicated geomagnetic satellite missions pro-

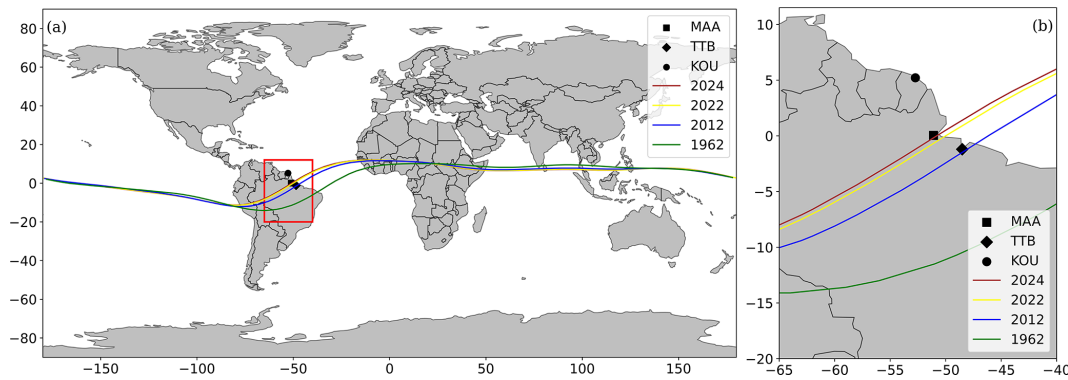


Figure 1. Magnetic equator calculated by the IGRF-13 (a) for 1 July of the following years: 1962 (green line), 2012 (blue line), 2022 (yellow line), and 2024 (red line). The zero-inclination lines are calculated considering 105 km altitude, the region where the equatorial electrojet is produced. In (b) a zoomed-in view of South America is shown, with the locations of Tatuoca (diamond), Kourou (circle), and Macapá indicated (square).

Tatuoca (TTB – island in Belém, PA), which have continuously measured the magnetic field since 1915 and 1957, respectively. There are two important magnetic phenomena in Brazil: the South Atlantic Anomaly (SAA), where the magnetic field intensity is the smallest globally, and the magnetic equator, where the magnetic inclination is zero.

In the last 60 years, the displacement of the magnetic equator in Brazil was the largest in the entire globe: 1100 km northwards, as predicted by the IGRF-13 (International Geomagnetic Reference Field) model (Alken et al., 2021). In Fig. 1 the magnetic equator is shown for different epochs in the last 60 years along with the forecast for 2024, where the secular variation of the inclination predicts the largest changes over Brazil (Alken et al., 2021). In this zero-inclination region, the magnetic field is mostly horizontal, and as a consequence strong ionospheric electric currents at about 105 km altitude are produced on the day side. These currents extend to about $\pm 3^\circ$ from the magnetic equator and are known as the equatorial electrojet (EEJ), as reviewed in Yamazaki and Maute (2017). The result is an intensification of the H -component daily variation (Soares et al., 2020), reaching up to about a 100 nT (see example in Fig. 2). In 2012, the magnetic equator passed over TTB, and its amplified diurnal variation was analysed by Soares et al. (2020). When compared to fields generated by solar quiet currents (Sq) from low and medium latitudes, the magnetic field in TTB shows a special variation influenced by the seasons, atmospheric oscillations, and lunar tides.

The magnetic equator continues to move northwards, and it is predicted by the IGRF-13 model (Alken et al., 2021) to be located at Macapá station at around July 2024 at Macapá station altitude (see Fig. 1). Therefore, a new magnetometer station was installed in Macapá in order to track the effects of the equatorial electrojet. This work is a result of a cooperation between Observatório Nacional (Rio de Janeiro, Brazil),

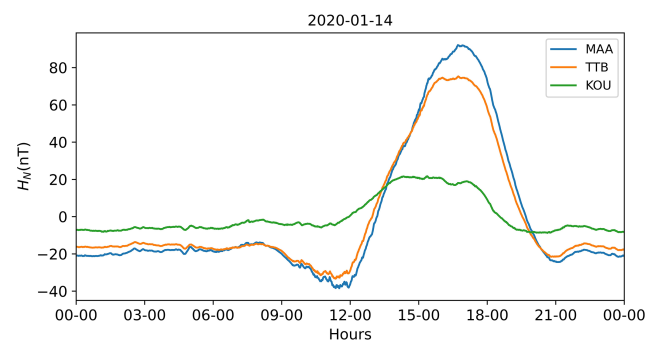


Figure 2. Comparison between the north-component daily variation of Tatuoca (TTB, 1.20° S, 48.51° W) and Kourou (KOU, 5.21° N, 52.73° W) magnetic observatories and the north component in the sensor coordinate system (H_N) of Macapá station on 14 January 2020. Local noon at TTB is 15:00 UTC.

Universidade Federal do Pará (UFPA, Brazil), and GFZ Potsdam (GFZ, German Research Center for Geosciences).

In order to choose the best location for Macapá station, two sites were tested in May 2019, i.e. at Chaves (0.180° N, 49.954° W, 2 m altitude) and at IEPA (Institute for Scientific and Technological Research of the State of Amapá, 0.038° S, 51.095° W, 34 m altitude). The total magnetic field was measured at both locations and 50 m to the north, south, east, and west of it. Since only a weak magnetic gradient of around 1 nT was found, the total field was measured for 3 consecutive days in both locations in order to check the data quality and possible noise from environmental interference. Both locations showed good data quality and good agreement with simultaneous TTB data. The access to Chaves is more difficult due to an 8 h trip by boat, while IEPA is more accessible. In addition, since IEPA is a public institution, local staff and infrastructure are available, which are both fundamental for the success of magnetometer stations in remote areas. Flux-gate magnetometers for measuring the components of the ge-

omagnetic field are temperature sensitive, and magnetometer stations typically do not have a temperature-controlled environment. Several methods have been used and published to first determine temperature coefficients of such magnetometers and then correct the recorded raw data (e.g. Janošek et al., 2018; Kudin et al., 2023).

2 Macapá station setup

In November 2019 the magnetometer station of Macapá (MAA) was installed on the IEPA campus (Fig. 3). There is no unique technique to install a magnetometer station since each location has its own requirements depending on the local conditions like weather, infrastructure, and staff availability. Two instruments measuring the magnetic field were installed in Macapá. A triaxial fluxgate magnetometer (GEOMAG-02 by Research Centre GEOMAGNET) measures the horizontal north (H_N), horizontal east (H_E), and vertical (Z) components (Appendix A) in the orthogonal sensor coordinate system. During the installation of the GEOMAG sensor set, we aligned it in a way that H_E is zero. The sampling rate is 1 Hz, and the time stamping is controlled by GPS and Network Time Protocol (NTP). The second instrument is a scalar Overhauser magnetometer (GSM-90 Overhauser by GEM Systems), which measures the scalar field strength F . The sampling rate is one sample every 5 s and NTP is used for the time stamping.

The GEOMAG sensor is installed inside a fibreglass shelter for protection against rain and wind (Fig. 3). This shelter has thermal insulation and is pyramid shaped (with a flat top; see Fig. 4), as was done for Tristan da Cunha observatory (Matzka et al., 2011). This design is similar but lighter than the pyramid described in Matzka et al. (2011). The foundation of the pyramid is made of concrete about 25 cm thick and 70 cm deep. The instrument pillar is also made out of concrete. It is completely separate from the pyramid foundation, about 60 cm \times 60 cm in cross section, 70 cm deep, and extends about 30 cm a.g.l. (above ground level). The fluxgate sensor is located directly on the concrete pillar and surrounded and covered by a Styrodur box with about 10 cm thickness. The GEOMAG electronics are in a box about 5 m from the pyramid (Fig. 4). The pyramid is located in the forest, around 70 m from the office building. Local staff assured us that in this region there is no flooding during the rainy season and that there are no fires during the dry season. To the east of the pyramid there are the buildings of the IEPA, and to the west the BioParque Amazonia, a newly opened attraction park and zoo, can be found. To the south, a larger street can be found about 300 m from the station.

3 Macapá dataset

Data from Macapá station (MAA) were recorded from 14 November 2019 until 25 July 2022 with an availability of 93 % for scalar data and 35 % for the vector data. The time distribution of the MAA dataset is shown in Fig. 5.

Since GEOMAG stopped transmitting data automatically via its serial RS-232 port on 5 December 2019, the data needed to be transferred by exchanging CF cards once a week. From this time on, the recording by the vector magnetometer had several interruptions due to technical problems such as damage to the GPS. Because of high temperatures in Macapá and insufficient shading of the electronics box, the GEOMAG-02 electronics inside it reached more than 50 °C, exceeding its maximum operating temperature of 40 °C as recommended by the manufacturer.

The GPS of the GEOMAG stopped working on 23 January 2021. This caused a time shift problem in the vector magnetic data (see example in Fig. 6). Since the GSM scalar data have correct time stamping, we could apply a correction to synchronise both signals. To do so, we apply the following sequence.

- i. Obtain a first approximation of the delay by finding for each day the time difference in the maxima in calculated F of the fluxgate and the measured F data of the Overhauser.
- ii. Systematically shift the time correction for the vector data, starting from the approximate delay found in (i) and calculating the correlation between the shifted calculated F data and the measured F data.
- iii. For each day, select the time stamp correction with the highest correlation.
- iv. For the whole period, perform a least-squares fitting using a spline on the selected time stamp corrections from (iii).
- v. The performed fitting will yield a smoothed time error correction for the whole period.

After synchronisation, we removed spikes and artificial disturbances from the data. Spike amplitudes exceeding 1 nT were removed. Spikes were detected by visually checking the first time derivative of each component. Artificial disturbance was visually identified in the geomagnetic data and its first time derivative and manually removed (see example in Fig. 7).

After the removal of spikes, MAA data were visually compared to TTB, showing a good agreement of H_N and H_E and a certain degree of anti-correlation in Z (Fig. 8), as is expected from the station location and the geometry of the equatorial ionospheric current system. Both TTB and MAA are under the influence of the EEJ (see Fig. 1), presenting a very similar effect of H -component amplification

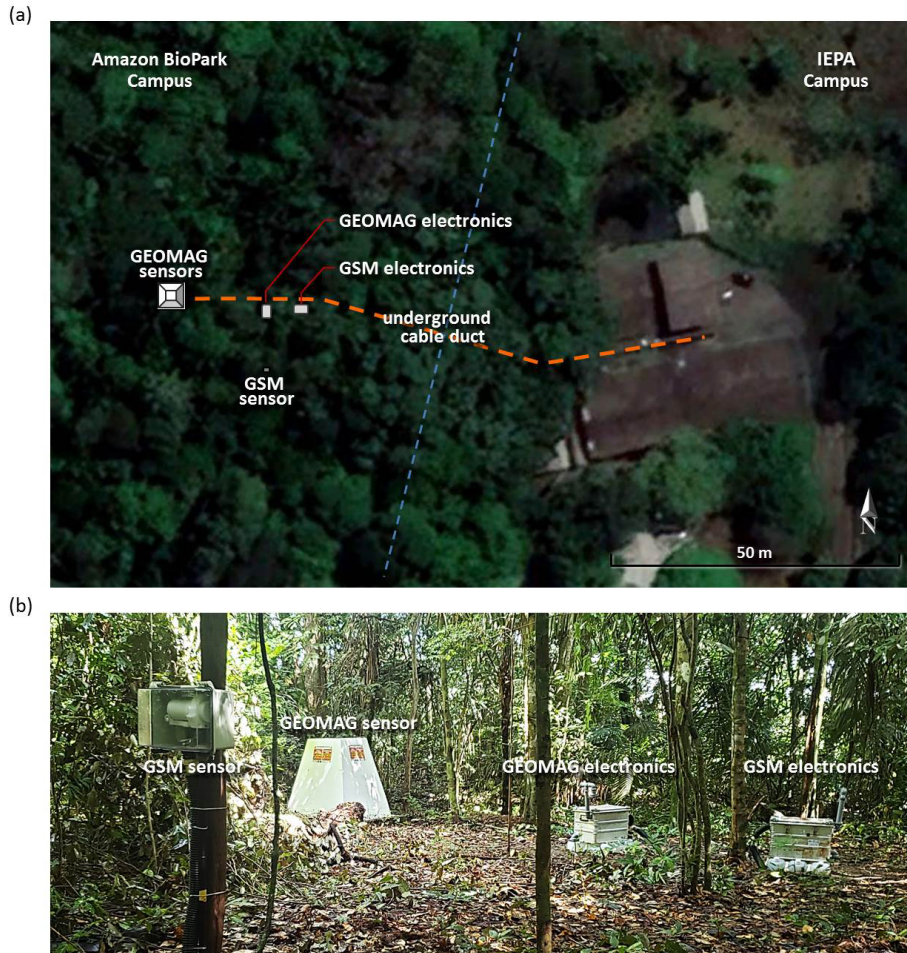


Figure 3. (a) Location of Macapá station (IEPA campus) showing the locations of the sensors and electronics. (b) An image of the fibreglass pyramid and the boxes with GEOMAG and GSM electronics.

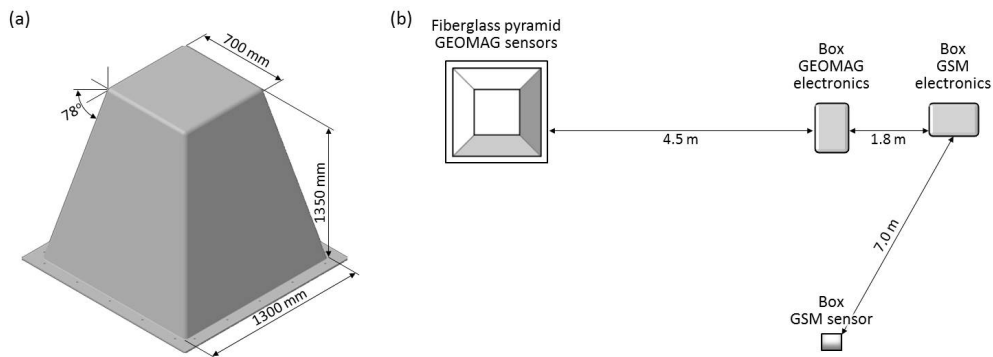


Figure 4. Fibreglass pyramid dimensions constructed for the Macapá magnetometer station (a) and schematic locations of the fibreglass pyramid with GEOMAG sensor, boxes with GEOMAG and GSM electronics, and the box with the GSM sensor (b).

(Fig. 8). Kourou (KOU) is the closest magnetic observatory from TTB, but it is still far from the magnetic equator and is therefore free from the effects of the EEJ. It is possible to isolate the localised EEJ effect from large-scale magnetospheric and large-scale solar quiet (Sq) signal by subtracting

the data of KOU from the MAA magnetometer station (see, e.g. Morschhauser et al., 2017; Soares et al., 2018). We calculated the differences between the horizontal components of MAA and KOU and TTB and KOU (Fig. 9). The differences indicate the intensity of the EEJ signal, which here is around

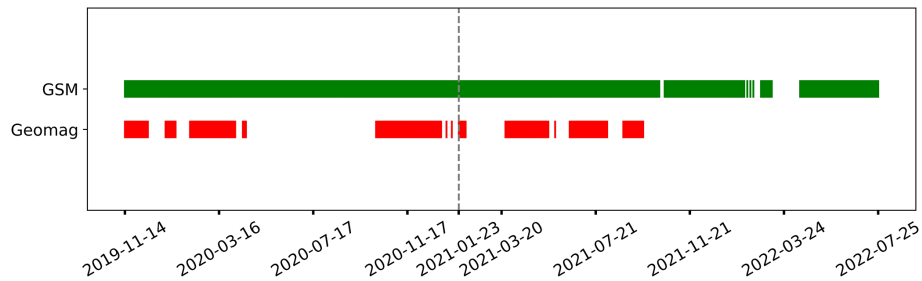


Figure 5. Temporal distribution of the scalar (GSM, green) and vector (GEOMAG, red) data available at the Macapá magnetometer station. The vertical dashed line indicates the starting time of the synchronisation problem.

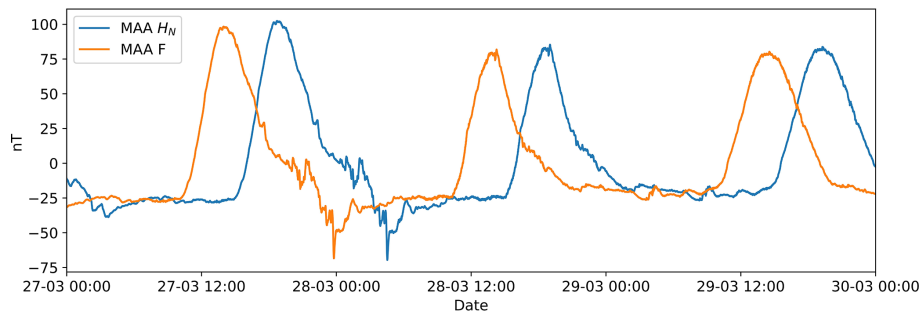


Figure 6. Example of a time shift caused by a GPS problem in Macapá station. The total field F was measured by the scalar magnetometer GSM and H_N by the vector magnetometer GEOMAG.

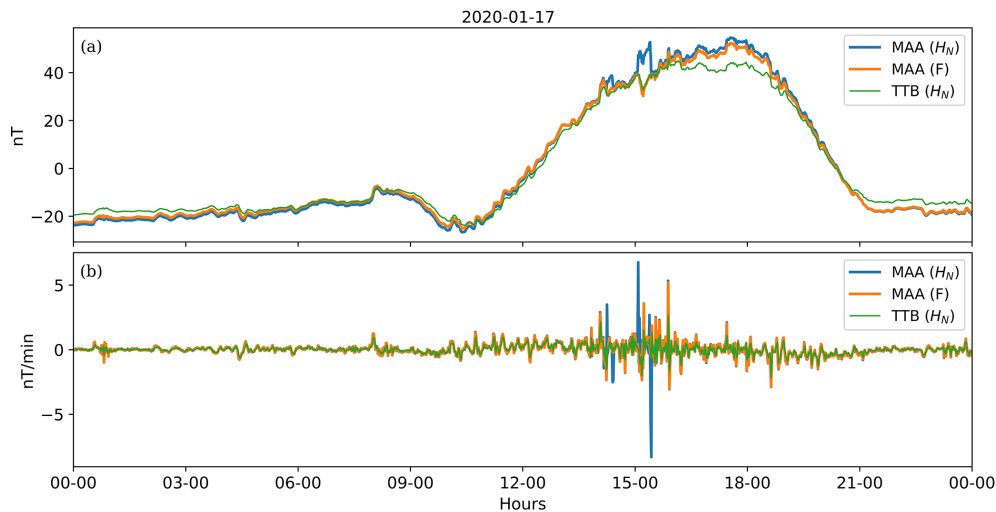


Figure 7. Example of artificial disturbance on 17 January (a) shown in H_N of MAA (blue line) compared to no disturbed signal in H_N of TTb (green line) and total field (F) at MAA (orange line). The first time derivative (b) of the H_N of MAA and TTb and F in MAA.

60 nT (peak to peak). Note that the difference for MAA is slightly greater than for TTb, indicating that the EEJ effect is slightly larger in MAA than in TTb.

4 Temperature correction

The total magnetic field is measured directly by the scalar magnetometer (here denoted as F_s , measured by GSM-90;

see Appendix A), which is assumed to be temperature invariant (Jankowski and Sucksdorff, 1996). It can also be calculated using the three components recorded by the vector magnetometer (here denoted as F_v , measured by GEOMAG). The temperature is measured in the pyramid (GEOMAG sensor, T_s) and in the box (GEOMAG electronics, T_e). Hourly mean values T_a of ambient temperature are measured by the Instituto Nacional de Meteorologia less than 2 km from the

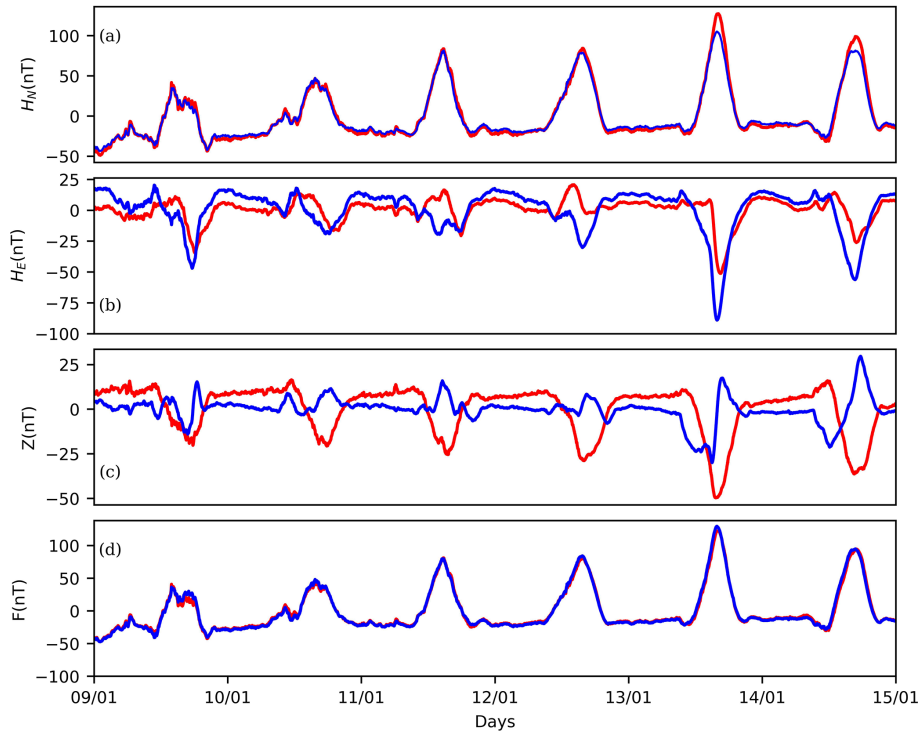


Figure 8. Comparison between the data of TTB (blue) and MAA (red) from 9–14 January 2020 for H_N (a), H_E (b), Z (c), and F (d).

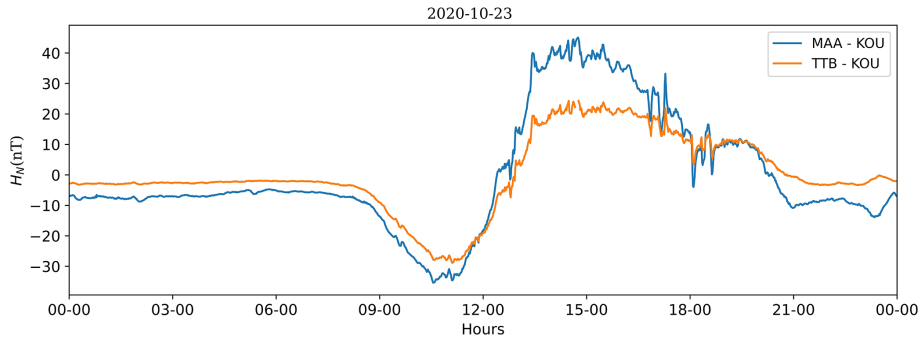


Figure 9. Differences between the horizontal components of Macapá (MAA) and Kourou (KOU) (blue line) and Tatuoca (TTB) and Kourou (brown line).

magnetometer station. All the variable and constant parameters used in this paper are listed in Appendix A. The electronic temperature is higher and more variable with time compared to sensor temperature (Fig. 10). They also show a time shift between the temperature peaks, which occur earlier in the electronics temperature. This happens because the electronics produce more heat and are less insulated from ambient temperature changes. Figure 10 shows the two temperature signals varying with time.

The calculated total field (F_v , Appendix A) using the three vector components is obtained by

$$F_v(t) = \left[(H_{N_0} + H_N(t))^2 + H_E(t)^2 + (Z_0 + Z(t))^2 \right]^{0.5}, \quad (1)$$

where t is time and H_{N_0} and Z_0 are the sensor offsets (also called baselines) of the north sensor and the vertical sensor, respectively. Note that the east sensor has a negligible small offset, which we set to 0 here. The baselines H_{N_0} was obtained by subtracting a typical value of H_N during nighttime and during quiet geomagnetic conditions from the simultaneous H value determined by the IGRF-13 model for the location of Macapá. The baseline Z_0 was determined in an analogue fashion. The difference between the calculated (F_v) and the observed scalar (F_s) total fields is denoted as follows:

$$\Delta F_0(t) = F_v(t) - F_s(t). \quad (2)$$

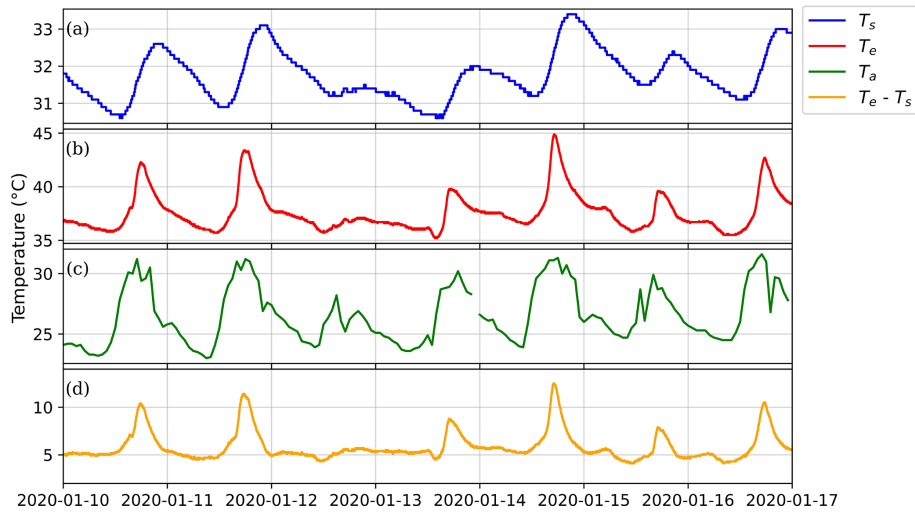


Figure 10. Temperature variation of the GEOMAG sensor (a), GEOMAG electronics (b), and ambient temperature (c) and the difference between temperature of the GEOMAG electronics and the sensor (d). The temperature variations are shown for 10–16 January 2020.

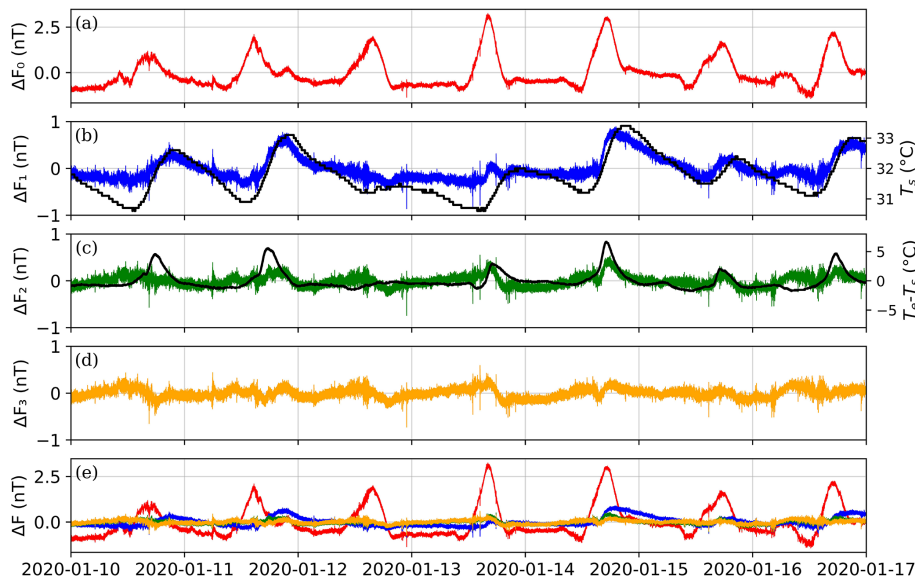


Figure 11. Macapá magnetometer station differences (ΔF_0 to ΔF_3) between the calculated total fields (F_{V_0} to F_{V_3}) and the scalar total field (F_S), from (a)–(d), respectively. In (b) and (c) the left y axis corresponds to ΔF_v , while the right y axis corresponds to the sensor temperature in b and to the difference in the electronics and sensor temperatures in c. All the ΔF_v values are plotted together in (e). The period shown in this example is from 10–17 January 2020.

This difference should be zero if both instruments perform their measurements correctly. But for Macapá station setup it varies with a daily periodicity, as exemplified in Fig. 11a. In order to obtain a possible scaling factor a_1 and offset b_1 between both signals, we minimise using least squares:

$$\min |\Delta F_0(t)| = \left[\sum_{t=1}^M ((a_1 F_v(t) + b_2) - F_s(t))^2 \right]^{0.5} \sim 0, \quad (3)$$

and we determine the coefficients by linear regression. We apply this correction to 5 d moving window for all MAA data

(The MathWorks Inc., 2018). We found that a_1 values are 0.964 ± 0.015 and that b_1 is negligible ($\sim 10^{-4}$ nT).

$$\Delta F_1(t) = F_{v_1}(t) - F_s(t) \quad (4)$$

The above equation still contains a periodic signal that is correlated to the sensor temperature (T_s), as shown in Figs. 11b and 12.

There is no significant temperature variation between 12 and 13 January 2020 (Fig. 10). However, in the same days the ΔF_0 varies with time (Fig. 11a), indicating that there is a

diurnal geomagnetic variation besides temperature variation. In order to remove the T_e signal, we minimised ΔF_1 and obtain the a_2 coefficient via linear regression (Appendix A):

$$\min|\Delta F_1(t)| = \left[\sum_{t=1}^M ((F_{v_1}(t) - a_2 T_s(t) + b_2) - F_s(t))^2 \right]^{0.5} \sim 0, \quad (5)$$

where typical values of a_2 are $-0.3 \pm 0.15 \text{ nT } ^\circ\text{C}^{-1}$ and b_2 is negligible ($\sim 10^{-9} \text{ nT}$) in all datasets. We expected that $F_{v_2}(t) = F_s(t)$, where $F_{v_2}(t) = F_{v_1}(t) - a_2 T_s(t)$. However,

$$\Delta F_2(t) = F_{v_2}(t) - F_s(t), \quad (6)$$

is still a periodic signal strongly correlated to the difference between the electronic temperature (T_e) and sensor temperature (T_s), as exemplified in Fig. 11. In order to remove the $T_e - T_s$ signal, we minimised ΔF_2 and obtain the a_3 coefficient via linear regression:

$$\min|\Delta F_2(t)| = \left[\sum_{t=1}^M (F_{v_2}(t) - a_3 (T_e(t) - T_s(t) + b_3) - F_s(t))^2 \right]^{0.5} \sim 0, \quad (7)$$

where a_3 typical values are -0.04 ± 0.025 and b_3 is also negligible ($\sim 10^{-12} \text{ nT}$) for all datasets. Therefore,

$$\Delta F_3(t) = F_{v_3}(t) - F_s(t) \sim 0, \quad (8)$$

where $F_{v_3}(t) = F_{v_2}(t) - a_3 (T_e(t) - T_s(t))$. Finally, the complete expression for the corrected calculated total field value F_v is as follows:

$$\tilde{F}_v(t) = a_1 F_v(t) - a_2 T_s(t) - a_3 (T_e(t) - T_s(t)), \quad (9)$$

which can be rewritten as

$$\tilde{F}_v(t) = a_1 F_v(t) - (a_2 - a_3) T_s(t) - a_3 T_e(t), \quad (10)$$

which is the more classical form of describing the temperature dependency of a magnetometer as it assigns a coefficient to the sensor temperature and the electronics temperature. In addition, INTERMAGNET suggests to monitor both sensor and electronics temperatures and to use these values for correction purposes (St-Louis et al., 2020, p. 10 and 11).

The critical point is that the sensor and electronics temperatures both depend on the ambient temperature. Therefore, they are not independent, and at the same time they do not have the same shape (Fig. 10a and b). This is because they have different insulation that creates a delay in the temperature maximum. After the correction of T_s , we remove part of the dependency on T_e , but there is still a signal corresponding to the difference between the temperatures (Fig. 10d) that needs to be removed. Now we can

compare the observed temperature coefficients (typical values are $a_2 = -0.3 \pm 0.15 \text{ nT } ^\circ\text{C}^{-1}$ and $a_3 = -0.04 \pm 0.025$) with the temperature coefficient given by the manufacturer. If the sensor and electronics are operating at the same temperature, the observed temperature coefficient will be around $a_2 = -0.3 \pm 0.15 \text{ nT } ^\circ\text{C}^{-1}$. This is close to the instrument specification of $< 0.2 \text{ nT } ^\circ\text{C}^{-1}$ given by the manufacturer for the GEOMAG-02 fluxgate.

It should also be noted that in the Macapá setup T_s and T_e remain different due to other factors like uneven sun exposure on the pyramid and on the box. This occurs because of the different shading by trees (albedo). Another factor is self-heating of the electronics, which is assumed to be a constant temperature change. We analyse the correlation between the different temperature signals with F_s to confirm the most appropriate correction sequence, as shown in Fig. 12a. Figure 12b quantifies how the misfit between F_s and the different F_v decreases with each correction. It would be preferable to determine a temperature coefficient for each of the three sensors of the GEOMAG-02. However, due to the location at the geomagnetic equator and because the instrument is oriented along magnetic north, the temporal change measured by the north sensor H_N corresponds very closely to the temporal change measured by the scalar magnetometer. At the same time, both H_E and $Z_0 + Z$ measure very small magnetic fields and hardly contribute to F_v . Therefore, the temperature coefficients determined here can be attributed to the H_N sensor, while the temperature coefficients of the H_E and Z sensor remain undetermined.

5 Conclusions

In this paper, we presented the new magnetometer station in Macapá (northern Brazil) built as a result of collaboration between the National Observatory (ON – Brazil), the Federal University of Pará (UFPA – Brazil), and the German Research Centre for Geosciences (GFZ – Germany). Macapá station is especially relevant because of the rapid temporal variation of the magnetic equator in the Brazilian longitudinal sector. The magnetic equator passed over Tatuoca observatory (TTB) in 2012 and continued to move northwards. Today it is located between Macapá station and Tatuoca observatory (Fig. 1). The IGRF model forecasts that the magnetic equator will continue to move northwards and pass by Macapá station in 2024. The presence of the magnetic equator causes another phenomena called the equatorial electrojet (EEJ), responsible for H -component amplification. Since Kourou magnetic observatory is out of the influence of the EEJ, it does not record the H -amplification, as it is observed in Tatuoca magnetic observatory (Fig. 2) and Macapá station.

At Macapá station we measured the total magnetic field (F) with a scalar magnetometer (GSM) and the three components (H_N , H_E and Z) with a vector magnetometer (GEOMAG). The sensor and electronics for each magne-

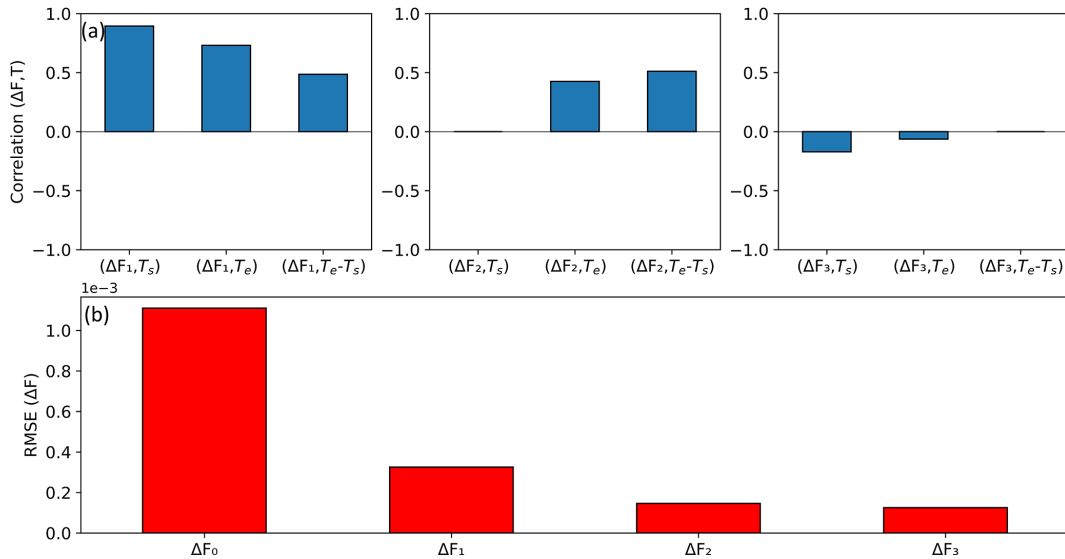


Figure 12. Correlation of ΔF_1 (left panel), ΔF_2 (middle panel), and ΔF_3 (right panel) with sensor temperature T_s , electronics temperature T_e , and $T_e - T_s$ in blue in (a). RMSE (root-mean-square error) for each ΔF is given in (b).

tometer were installed in different huts (Fig. 3). The GEOMAG sensor was inside a fibreglass pyramid about 5 m from the electronics box (Fig. 4). We recorded data from Macapá station from November 2019 until September 2021 (Fig. 5). There were some problems in the data acquisition, such as a GPS failure that caused a time shift between the data of GEOMAG and GSM (Fig. 6). The time shift and other problems in the data, such as noise and spikes (example in Fig. 7), were corrected. Macapá data were then compared with TTb, which is the closest observatory. The data of TTb and Macapá showed good agreement (Fig. 8), which helps to assure the quality of the recorded data.

In order to measure the amplitude of the equatorial electrojet (EEJ), we subtract the data from Macapá station and TTb, both under the influence of the EEJ, from Kourou observatory (Fig. 9). The EEJ signal was recorded at Macapá with a similar amplitude to that at TTb.

Because of the particular setup configuration of Macapá (Fig. 3), we got very different values for the temperature of the (GEOMAG) sensor and electronics (Fig. 10), and presumably these temperature variations influence the Macapá data. We implement a methodology considering two types of correction in the data: diurnal variation (between GEOMAG and GSM – included in ΔF_0) and temperature variation (included in ΔF_1 and ΔF_2), as shown in Fig. 11. The results demonstrate that there is a high correlation between the difference in GEOMAG and GSM with the temperature of the sensor and electronics and the difference between them (Fig. 12). Therefore, it is important to consider that variations in temperature may affect the data of magnetic stations, and it may be important to apply a correction.

Appendix A: Notation used in this paper for each variable and constant parameters

Notation	Description
$F_s(t)$	Observed scalar total field recorded by the GSM
$H_N(t)$	Horizontal north magnetic field in the sensor coordinate system
$H_E(t)$	Horizontal east magnetic field in the sensor coordinate system
$Z(t)$	Vertical magnetic field
$T_e(t)$	Electronic temperature measured inside the box (GEOMAG)
$T_s(t)$	Sensor temperature measured inside the pyramid (GEOMAG)
$T_a(t)$	Ambient temperature of Macapá station
$F_v(t)$	Calculated total field using the three vector components of GEOMAG
$F_{v_1}(t)$	$F_v(t)$ corrected by linear regression using $F_s(t)$
$F_{v_2}(t)$	$F_{v_1}(t)$ corrected by linear regression using $T_s(t)$
$F_{v_3}(t)$	$F_{v_2}(t)$ corrected by linear regression using $(T_e(t) - T_s(t))$
$\tilde{F}_v(t)$	Corrected calculated total field value (final)
$\Delta F_0(t)$	Difference between $F_v(t)$ and $F_s(t)$
$\Delta F_{1-3}(t)$	Differences between $F_{v_{1-3}}(t)$ and $F_s(t)$
$(a, b)_{1-3}$	Linear regression coefficients
H_{N_0}	Baseline value of the horizontal component calculated by the IGRF model
Z_0	Baseline value of the vertical component calculated by the IGRF model

Code availability. The minimization to obtain the values of a_s and b_s was done with the MATLAB POLYFIT function, using as input the curves for which we want to minimize the difference, selecting degree one for linear regression. The output of this POLYFIT function is the angular and linear coefficients, respectively, the a_s and b_s of Eqs. (3), (5) and (7) (<https://www.mathworks.com>, The MathWorks Inc., 2018).

Data availability. The dataset is available at <https://doi.org/10.5880/GFZ.2.3.2024.002> (Da Silva et al., 2024).

Author contributions. CMM installed Macapá station and performed the measurements and the computations. AM and JM planned the design of Macapá station. CMM, KJP, and JM drafted the manuscript. MVS and RPC designed the figures. All authors discussed the results and commented on the manuscript.

Competing interests. The contact author has declared that none of the authors has any competing interests.

Disclaimer. Publisher's note: Copernicus Publications remains neutral with regard to jurisdictional claims made in the text, published maps, institutional affiliations, or any other geographical representation in this paper. While Copernicus Publications makes every effort to include appropriate place names, the final responsibility lies with the authors.

Special issue statement. This article is part of the special issue "Geomagnetic observatories, their data, and the application of their data". It is a result of the XIXth IAGA workshop on Geomagnetic Observatory Instruments, Data Acquisition and Processing, Sopron and Tihany, Hungary, 22–26 May 2023.

Acknowledgements. We would like to thank IEPA for the support regarding work at Macapá station, including the installation and availability of infrastructure and sourcing of local staff. We also thank BioParque Amazônia for providing the space to install the instruments and IMET for the ambient temperature data.

Financial support. Katia Jasbinschek Pinheiro received financial support from CNPq (Bolsa de Produtividade em Pesquisa – 306538/2022-9).

The article processing charges for this open-access publication were covered by the Helmholtz Centre Potsdam – GFZ German Research Centre for Geosciences.

Review statement. This paper was edited by Daniel Kastinen and reviewed by Jan Reda, Anatoly Soloviev, Anna Willer, and one anonymous referee.

References

- Alken, P., Thébaud, E., Beggan, C. D., Amit, H., Aubert, J., Baerenzung, J., Bondar, T. N., Brown, W. J., Califf, S., Chambodut, A., Chulliat, A., Cox, G., Finlay, C. C., Fournier, A., Gillet, N., Grayver, A., Hammer, M. D., Holschneider, M., Huder, L., Hulot, G., Jager, T., Kloss, C., Korte, M., Kuang, W., Kuvshinov, A., Langlais, B., Léger, J.-M., Lesur, V., Livermore, P. W., Lowes, F. J., Macmillan, S., Mages, W., Manda, M., Marsal, S., Matzka, J., Metman, M. C., Minami, T., Morschhauser, A., Mound, J. E., Nair, M., Nakano, S., Olsen, N., Pavón-Carrasco, F. J., Petrov, V. G., Ropp, G., Rother, M., Sabaka, T. J., Sanchez, S., Saturnino, D., Schnepf, N. R., Shen, X., Stolle, C., Tangborn, A., Tøffner-Clausen, L., Toh, H., Torta, J. M., Varner, J., Vervelidou, F., Vigneron, P., Wardinski, I., Wicht, J., Woods, A., Yang, Y., Zeren, Z., and Zhou, B.: International Geomagnetic Reference Field: the thirteenth generation, *Earth Planets Space*, 73, 1–25, <https://doi.org/10.1186/s40623-020-01288-x>, 2021.
- Chulliat, A., Matzka, J., Masson, A., and Milan, S.: Key ground-based and space-based assets to disentangle magnetic field sources in the Earth's environment, *Space Sci. Rev.*, 206, 123–156, <https://doi.org/10.1007/s11214-016-0291-y>, 2017.
- Da Silva, M. V., Matzka, J., Mendel Martins, C., Jasbinschek Pinheiro, K., Ohlert, A., Silverio Bernardes, V., Bronkalla, O., Haseloff, J., Rettig, S., and Seeger, T.: Magnetometer station Macapa, Brazil, calibrated 1-second geomagnetic data, V.1, GFZ Data Services [data set], <https://doi.org/10.5880/GFZ.2.3.2024.002>, 2024.
- Hulot, G., Finlay, C. C., Constable, C. G., Olsen, N., and Manda, M.: The Magnetic Field of Planet Earth, *Space Sci. Rev.*, 152, 159–222, <https://doi.org/10.1007/s11214-010-9644-0>, 2010.
- Jankowski, J. and Sucksdorff, C.: Guide for Magnetic Measurements and Observatory Practice, International Association of Geomagnetism and Aeronomy, Warsaw, 235 pp., ISBN 0-9650686-2-5, 1996.
- Janošek, M., Butta, M., Vlk, M., and Bayer, T.: Improving Earth's Magnetic Field Measurements by Numerical Corrections of Thermal Drifts and Man-Made Disturbances, *J. Sensors*, 2018, 1–10, <https://doi.org/10.1155/2018/1804092>, 2018.
- Kudin, D., Soloviev, A., Matveev, M., and Shevaldysheva, O.: On a Novel Approach to Correcting Temperature Dependencies in Magnetic Observatory Data, *Appl. Sci.*, 13, 8008, <https://doi.org/10.3390/app13148008>, 2023.
- Matzka, J., Chulliat, C., Manda, M., Finlay, C. C., and Qamili, E.: Geomagnetic Observations for Main Field Studies: From Ground to Space, *Space Sci. Rev.*, 155, 29–64, <https://doi.org/10.1007/s11214-010-9693-4>, 2010.
- Matzka, J., Husoy, B.-O., Berarducci, A., Wright, D., Pedersen, L. W., Stolle, C., Repetto, R., Genin, L., Merenyi, L., and Green, J. J.: The geomagnetic observatory on Tristan da Cunha: Setup, operation and experiences, *Data Sci. J.*, 10, 367–376, <https://doi.org/10.2481/dsj.IAGA-22>, 2011.
- Morschhauser, A., Brando Soares, G., Haseloff, J., Bronkalla, O., Protásio, J., Pinheiro, K., and Matzka, J.: The magnetic ob-

- servatory on Tatuoca, Belém, Brazil: history and recent developments, *Geosci. Instrum. Method. Data Syst.*, 6, 367–376, <https://doi.org/10.5194/gi-6-367-2017>, 2017.
- Soares, G., Yamazaki, Y., Matzka, J., Pinheiro, K., Morschhauser, A., Stolle, C., and Alken, P.: Equatorial Counter Electrojet Longitudinal and Seasonal Variability in the American Sector, *J. Geophys. Res.-Space*, 123, 9906–9920, <https://doi.org/10.1029/2018JA025968>, 2018.
- Soares, G., Yamazaki, Y., Cnossen, I., Matzka, J., Pinheiro, K. J., Morschhauser, A., Alken, P., and Stolle, C.: Evolution of the Geomagnetic Daily Variation at Tatuoca, Brazil, From 1957 to 2019: A Transition From Sq to EEJ, *J. Geophys. Res.-Space* 125, 1–20, <https://doi.org/10.1029/2020JA028109>, 2020.
- St-Louis, B., INTERMAGNET Operations Committee, and INTERMAGNET Executive Council: INTERMAGNET Technical Reference Manual, Version 5.0.0 (INTERMAGNET), GFZ Data Services, Potsdam, p. 146, <https://doi.org/10.48440/INTERMAGNET.2020.001>, 2020.
- The MathWorks Inc.: MATLAB version: 9.4.0 (R2018b), The MathWorks Inc., Natick, Massachusetts, USA, <https://www.mathworks.com> (last access: 20 September 2024), 2018.
- Yamazaki, Y. and Maute, A.: Sq and EEJ – A Review on the Daily Variation of the Geomagnetic Field Caused by Ionospheric Dynamo Currents, *Space Sci. Rev.*, 206, 1–107, <https://doi.org/10.1007/s11214-016-0282-z>, 2017.